Acta of Bioengineering and Biomechanics
Vol. 21, No. 2, 2019

Original paper
DOI: 10.5277/ABB-01294-2019-02

Mechanical response at peri-implant mandibular bone for variation of pore characteristics of implants: A Finite Element Study

SULAGNA SARKAR[1], TIKESHWAR PRASAD SAHU[2], ARIJIT DATTA[2], NIMESH CHANDRA[2], ARINDAM CHAKRABORTY[2], PALLAB DATTA[3], SANTANU MAJUMDER[2]*, AMIT ROY CHOWDHURY[2]

[1] Department of Metallurgical and Material Engineering, Jadavpur University, India.
[2] Department of Aerospace Engineering and Applied Mechanics,
Indian Institute of Engineering Science and Technology, Shibpur, India.
[3] Centre for Healthcare Science and Technology,
Indian Institute of Engineering Science and Technology, Shibpur, India.

Purpose: In this paper, the mechanical response of generic dental implants having calculated porosities with varying pore-sizes has been evaluated. The purpose of this study was to compare the developed stress-strain of designed porous implants (i.e., stress at the implant and strain at the peri-implant bone) with that of the non-porous implant. *Methods:* 3D model of a mandible was prepared from CT scan data and nine generic dental implant models have been designed having 10%, 20%, and 30% porosity with 500, 700, and 900 micron pore size along with a non-porous model for carrying out FE analyses. First, failure analyses of implants, under a biting force of 250 N have been performed. Next, the remaining implants have been further evaluated under average compressive chewing load of 100 N, for mechanical responses at bone-implant interface. *Results:* Von Mises strain at the peri-implant mandibular bone increases with the increase in percentage porosity of the implant material and maximum implant stress remained much below the yield stress level. *Conclusion:* Implant stiffness and compressive strength vary as a function of porosity and pore size. Strain obtained on the peri-implant bone is sufficient enough to facilitate better bone growth with the 700 micron pore size and 30% porosity, thus reducing the effect of stress shielding.

Key words: *porous dental implant, pore size, percentage porosity, bone-implant interface, finite element analysis, stress and strain*

1. Introduction

Dental implants are paramount to the treatment of edentulous jaw, allowing for a permanent solution for replacing missing teeth. This surgical technique offers rehabilitation of either partial or total-edentulous jaws [3], [5]. Titanium and its alloys (Ti-6Al-4V) are one of the most preferred biomaterials for orthopaedic and dental implants due to their desirable mechanical properties, excellent corrosion resistance, and compatible biological properties [16], [1].

Implants are often accompanied by serious complications, such as aseptic loosening, caused by micro motion of the prosthesis due to insufficient initial fixation and septic loosening due to implant-associated infections [19]. Problems such as loosening and premature failure of the implant arise due to the difference of stiffness between implant and bone ($E_{\text{Ti-6Al-4V}}$ = 110–120 GPa versus E_{bone} = 10–30 GPa) [24], [2]. The mismatch causes the peri-implant bone to suffer from stress-shielding and insufficient loading. A potential risk to the long term stability of the designed implant is caused due to the resorption of the

* Corresponding author: Santanu Majumder, Department of Aerospace Engineering and Applied Mechanics, Indian Institute of Engineering Science and Technology, Shibpur, IIEST, Shibpur, 711103, Howrah, India. Phone: +91-33-2668 4561, e-mail: majumder.santanu@gmail.com
Received: January 11th, 2019
Accepted for publication: May 9th, 2019

bone tissue [2], [10]. There are a few critical factors in the bone remodelling stage of osseointegration, which takes a typical healing period of around 3–6 months. The most important factor is the extent of contact between bone and implant along the bone-implant interface. The other factors are magnitude and direction of the forces acting along the implant, and the contour shape of the implant. To overcome the problem of stress-shielding, two things are commonly proposed, (i) development of low modulus alloys and (ii) reduction of the stiffness with the help of incorporation of porosity [17], [8], [13], [18]. The porous titanium implants have certain advantages over the non-porous ones. Porosity increases surface area, lowers the stiffness, promotes vascularisation and bone in-growth leading to enhanced stability at the bone-implant interface [13], [18], [15]. However, high porosities can cause intense stress localization (stress concentration) in the implant around the pore periphery and can lead to the reduction of the mechanical strength, a cause of serious concern [15].

To accomplish the required mechanical properties by controlling porosity, proper pore characteristics of Ti or Ti-based alloys is needed for customized implant designing [23], [11]. If the mechanical properties of such porous body are predicted with high reliability by computer simulation process using finite element (FE) analysis, the results can be used in designing the customized implants in short time. Roy et al. [20] designed cylindrical porous titanium dental implants with non-helical thread and concluded that porous implants generated better stress–strain characteristics at the peri-implant bone with varying bone conditions. Moreover, to achieve functionally graded materials properties, porosity can also be changed from location to location to attain optimum bone-implant interface strain [14].

Considering tapered implant with helical thread, the objective of this FE analysis is to depict strain distribution at the peri-implant mandibular bone as well as stress distribution at the dental implant for different pore size and % porosity under compressive load, and compare them with the non-porous implant.

2. Material and methods

2.1. Three-dimensional (3D) model of mandible

Computed tomography (CT) scan data of mandibular bone was collected in the DICOM (0.208 × 0.208 × 2.0) format, provided by CMERI, Durgapur. Contours were generated using a threshold value of 600 Hounsfield unit (HU). CT slices were processed in MIMICS® image processing software. After the segmentation process, a 3D solid model of mandible was created and the molar portion of the mandible was selected (Fig. 1a).

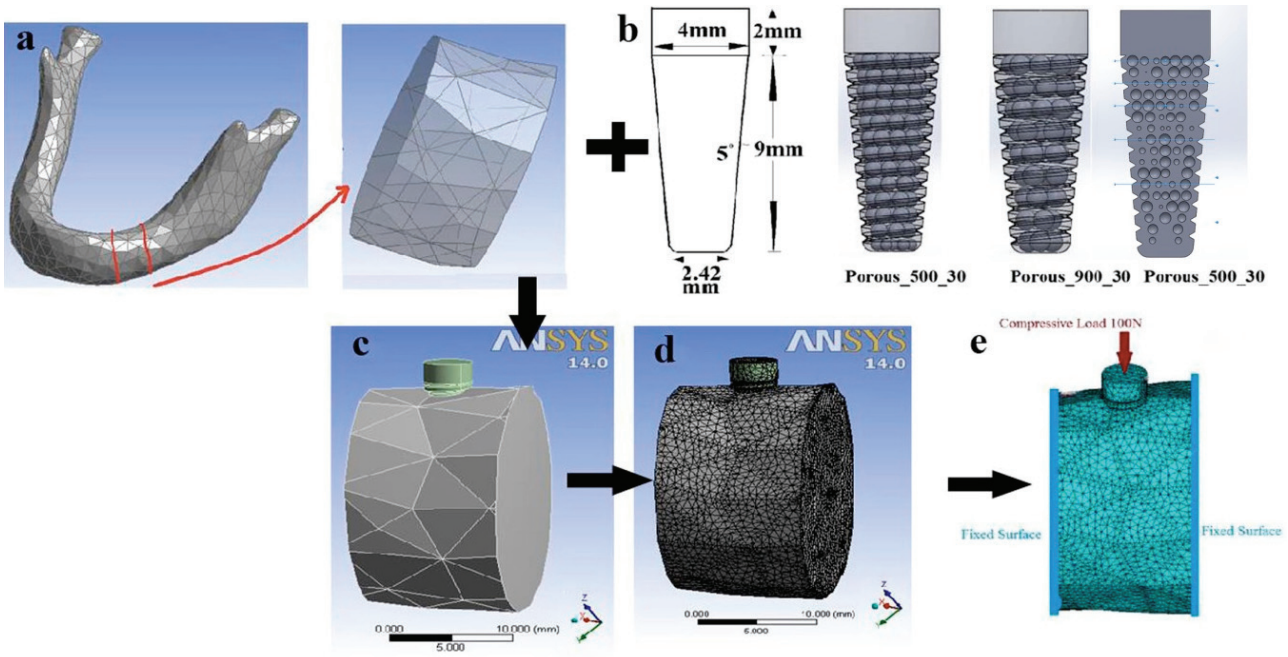

Fig. 1. (a) Selection of bone sample, for implant placement, from the molar region of mandible, (b) geometry of porous implant and two porous models; (c) assembly of implant and part of mandible; (d) meshed assembly; (e) meshed mandible-implant assembly with compressive loading and the boundary condition

2.2. Design of implant

A solid implant with 5° tapering and helical thread has been designed in Solid Works® software. The porous structures are created by introducing well-defined microspheres of 500, 700, and 900 micron in the solid implant with 10%, 20%, and 30% porosity. The spherical pores are positioned in parallel planes along the cross-section of the implant. A total 9 number of such models with varying porosity and pore size along with a non-porous one have been designed (Table 1). The geometry of the implant is shown in Fig. 1b.

Table 1. Nomenclature of implants according to pore specification

No.	Name	Pore size [μm]	Porosity [%]
1	Non-porous	0	0
2	Porous_900_10	900	10
3	Porous_900_20	900	20
4	Porous_900_30	900	30
5	Porous_700_10	700	10
6	Porous_700_20	700	20
7	Porous_700_30	700	30
8	Porous_500_10	500	10
9	Porous_500_20	500	20
10	Porous_500_30	500	30

2.3. Generation of FE model

The solid models of the implant and the molar portion of the mandible were imported into the ANSYS® FE analysis software and assembled together after generating the proper 3D co-ordinate system. Through boolean operation, the implant was inserted and assembled in the mandible, keeping one thread outside (Fig. 1c). Meshing of implant and the mandible was done with an element size of 0.05 mm and the surface where the load was to be applied had a meagre element size of 0.03 mm (Fig. 1d). For meshing, 10-noded tetrahedral elements have been used and convergence analyses were done by re-setting the element size until the difference was less than 2%. Frictional co-efficient 0.3 was used to connect the mandible and implant for the node-to-node frictional contact between elements [9].

2.4. Material property

Ti6Al4V was used as an implant material with Young's modulus of 114 GPa and Poisson's ratio of 0.3. Bone was considered as linear elastic and effectively non-homogeneous. As modulus of elasticity (E) for bone depends on bone density (ρ), which, in turn, depends on the value of bone HU, the following relation was used for calculation of ρ and E [12].

$$\rho = 0.000769*\text{HU} + 1.028, \quad (1)$$

$$E = 2349\,\rho^{2.15}. \quad (2)$$

For the mandibular bone, the HU threshold varies from 418 to 3071, the calculated ρ and E varied from 0.336 to 2.045 gm/cc and 224 to 10938 MPa, respectively. Poisson's ratio was taken as 0.3 [7].

2.5. Boundary condition and loading

The maximum biting force generated in molar teeth was in the range of 350 to 500 N [4]. Considering the average force is about 60% of the maximum force, a maximum compressive chewing load of 250 N was applied on the top most surface of the implants in a distributed manner to observe maximum implant stress. As yield stress of Ti6Al4V alloy is 970 MPa [20], only those implants where the maximum working stress generated in implant is below 450 MPa considering a factor of safety of 2 were considered for further analysis. Then, the average compressive chewing load of 100 N was applied to the implant in a distributed manner to observe the mechanical response at bone-implant interface as well as peri-implant bone (Fig. 1e) [7]. To provide the boundary conditions, the two lateral surfaces of the dissected mandible model were kept fixed.

3. Results

The FE analyses were carried out to observe the von Mises stress at implant and von Mises strain at the peri-implant bone during the application of the load. Under initial chewing load of 250 N, maximum von Mises stress values have not exceeded the 450 MPa. Further, a comparative study was done for porous implants with 10%, 20% and 30% porosity, along with a non-porous solid implant (0% porosity) under 100 N of average chewing load. Effect of porosity were to be compared within the 3 equivalent dental zones: cervical third, middle third and apical third. For this purpose, 11 positions (from top to bottom) have been selected on both the implant and peri-implant bone along the bone-implant interface, which were used to study the effect of porosity on both the implant and peri-implant bone in three anatomical sections (apical, middle, and cervical thirds) (Fig. 2).

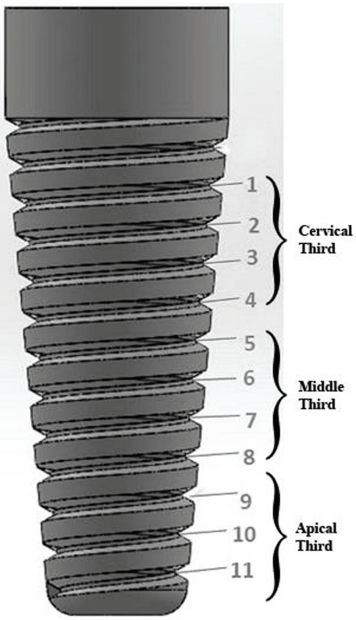

Fig. 2. Eleven positions within the implant along the bone-implant interface, equivalent to three dental zones: cervical third, middle third and apical third

3.1. Effect of variations of % porosity for 900 micron pore size

Within the implants, with the increase of percentage (%) porosity, the maximum von Mises stress increased distinctly for the positions 3, 5, 6, and 9 at the implant-bone interface (Fig. 3a). This was corroborated by a maximum stress of 140 MPa (position 1) for non-porous implant (0% porosity), as opposed to a stress of 260 MPa (position 3) being obtained for implant with 30% porosity. The minimum von Mises stress for all the cases (porous and non-porous) was about 63 MPa and was obtained at position 11.

Within the peri-implant bone, with the increase of % of porosity, von Mises strain distinctly increased along all the 11 positions at the implant-bone interface (Fig. 3b). This was substantiated by a maximum strain of 4000 micro-strain (position 5) for non-porous implants (0% porosity) versus 7100 micro-strain (position 11) for 30% porosity implant. The

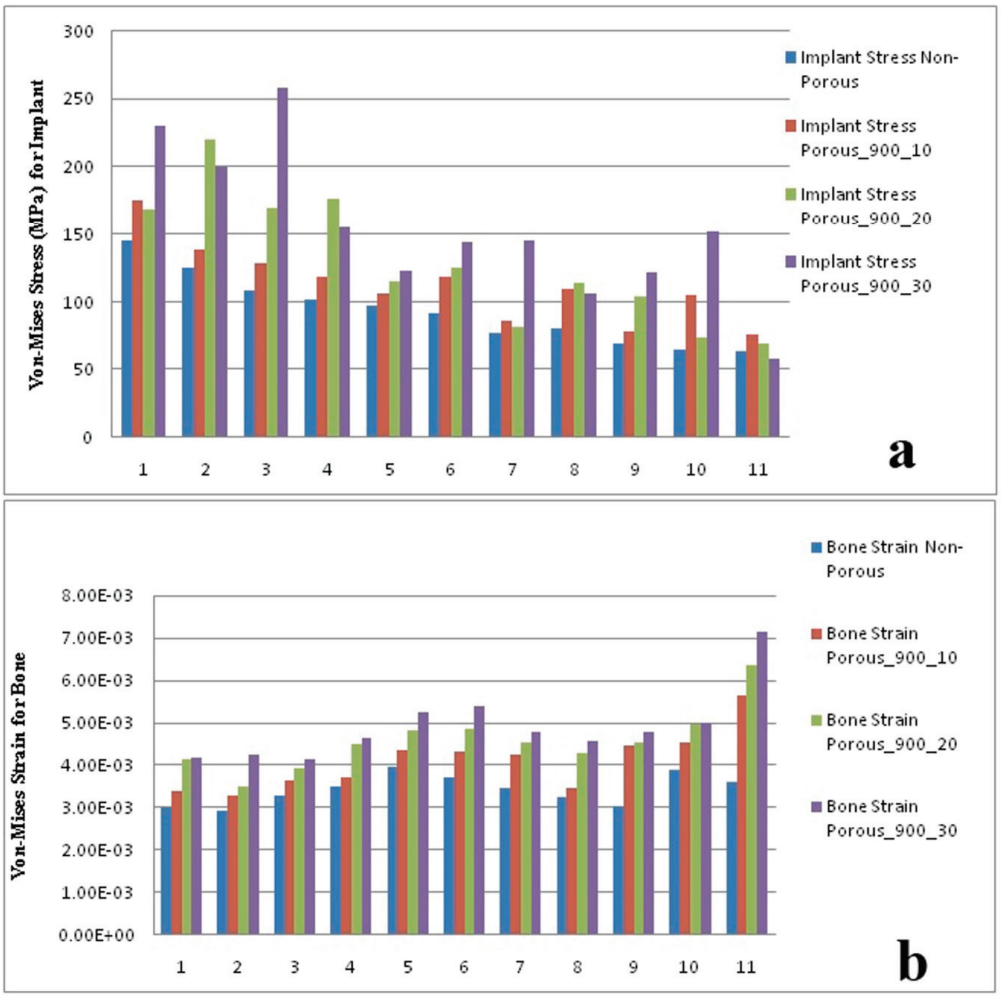

Fig. 3. For implant of 900 micron pore size and 0% (non-porous), 10%, 20% and 30% porosity at 11 locations along the implant-bone interface, (a) comparative von Mises stress within the implant and (b) comparative von Mises strain within the peri-implant bone

magnitude of the minimum von Mises strain increases with increased porosity (from 2900 micro-strain at position 2 for non-porous versus 4100 micro-strain at position 3 for 30% porosity).

3.2. Effect of variations of % porosity for 700 micron pore size

With the increase of % porosity, the maximum von Mises stress within the implant increases for the positions 3, 5, 7, 8, and 10 (Fig. 4a) along the implant-bone interface. Maximum stress of 140 MPa for non-porous implant, as opposed to the stress of 215 MPa for implant with 30% porosity validated this fact. As a result, the range of stress obtained for 700 micron pore size was lower than that of 900 micron pore size. High stress values were noted at position 3, irrespective of % porosity. The magnitude of minimum von Mises stress for all cases was uniform with an average of 66 MPa (position 11). Within the peri-implant bone, von Mises strain magnitude was found to increase with increasing % porosity at each 11 positions (Fig. 4b). Except for a few positions, the strain increased longitudinally along the bone, irrespective, of the % porosity.

3.3. Effect of variations of % porosity for 500 micron pore size

Similar trend was observed for implant von Mises stress (Fig. 5a) and von Mises strain for peri-implant bone (Fig. 5b). The range of stress obtained for 500 micron pore size was lower than that of 700 and 900 micron. Hereby, also high values stresses were observed at position 3, irrespective of % porosity. The magnitude of minimum von Mises stress for all % porosities was uniform with an average of 63 MPa and was obtained at position 11.

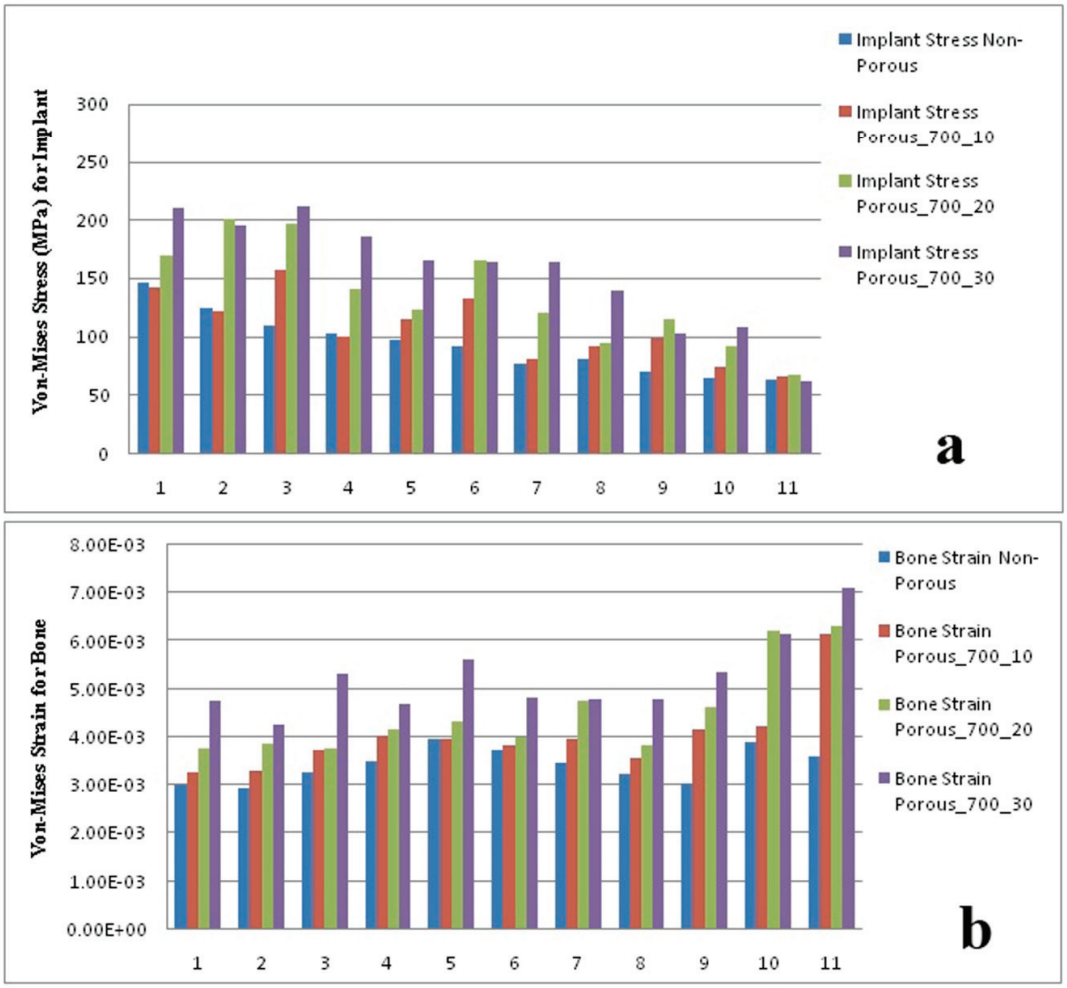

Fig. 4. For implant of 700 micron pore size and 0% (non-porous), 10%, 20% and 30% porosity at 11 locations along the implant-bone interface, (a) comparative von Mises stress within the implant and (b) comparative von Mises strain within the peri-implant bone

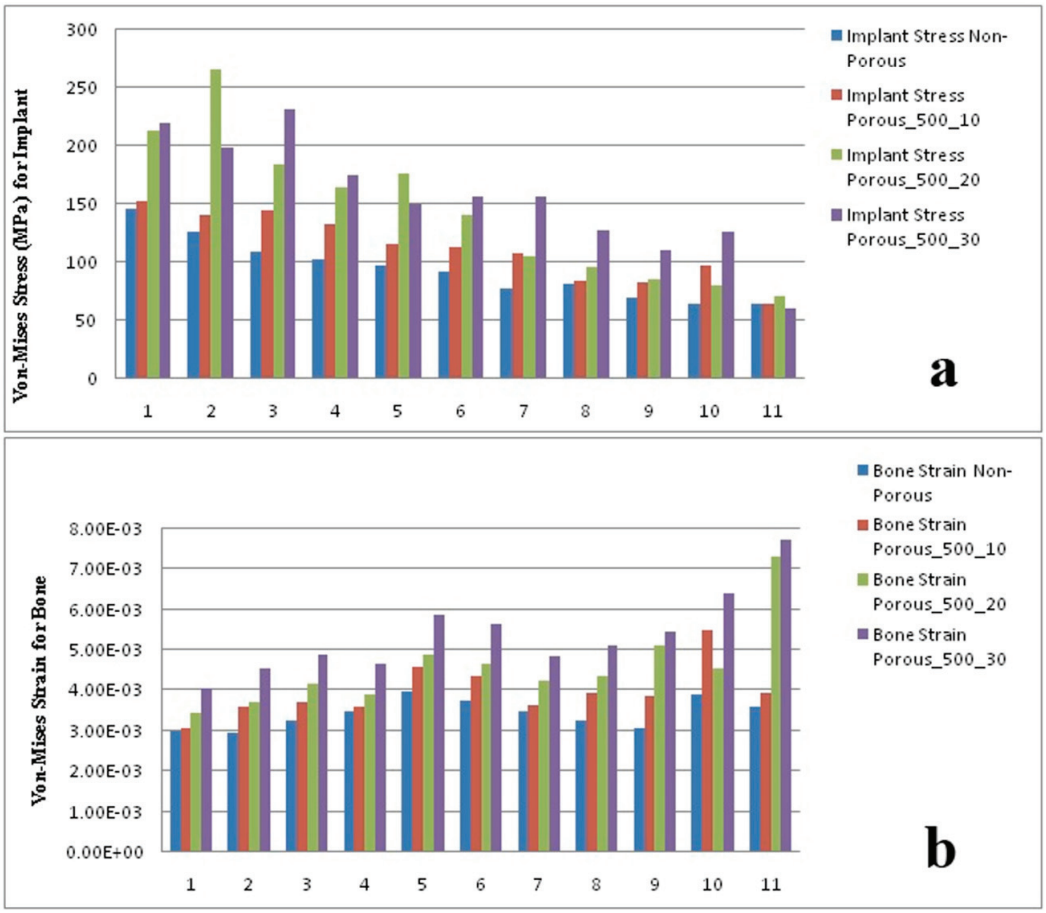

Fig. 5. For implant of 500 micron pore size and 0% (non-porous), 10%, 20% and 30% porosity at 11 locations along the implant-bone interface, (a) comparative von Mises stress within the implant and (b) comparative von Mises strain within the peri-implant bone

4. Discussion

FE analyses were performed under compressive load for 9 porous models and one non-porous model. The present study incorporated varying degrees of porosity, having 10, 20 and 30% porosity with 500, 700 and 900 micron pore size, to decrease the overall stiffness of the dental implant. Torres-Sanchez et al. [22] observed that pore size more than 300 micron exhibits the most favourable conditions for cell proliferation. Hence, pores of 500, 700 and 900 micron diameter were implemented in this study. Failure of implant may have occurred due to two reasons: mechanical fracture due to stiffness reduction with the incorporation of porosity, and aseptic loosening. Under the current loading condition, the generated maximum stress should be much below the yield limit of the implant material (970 MPa for Ti6Al4V; [20]). Porosity decreased the stiffness along the loading direction resulting in simultaneous increase in strain in the lateral direction. Hence, this phenomenon, in turn, introduced a higher strain in the surrounding bone tissues to combat stress shielding by promoting a greater bone apposition. Osseointegration, by generation of optimum strain at the adjacent bone, can prevent aseptic loosening. The magnitude of the desirable strain at the adjacent bone to implant should be around 3000–5000 micro-strain, which is comparable to the strain obtained for healthy natural tooth [22].

Among all the cases, the highest von Mises stress for the implant has been observed as 260 MPa at 30% porous implant with 900 micron pore size (noted at position 3, Fig. 3a). It occurred just adjacent to the porous hole. The yield strength of titanium alloy was about 970 MPa and it is obvious that the generated stresses in the implants were within the safety range. It was also observed that the stress values were significantly high in the cortical region, as opposed to low stress obtained in cancellous portion.

The distribution of strain depicted an increase of strain at the cancellous region (Fig. 3b). This was due the reason that the cancellous region is less stiff and is more susceptible to deformation. Also, the implant

stress was high adjacent to the cortical region, as shown in Fig. 3a, hence, the adjacent mandibular bone was also suffering from low strain. It was also observed that, in the case of non-porous implant, the bone adjacent to the implant suffered from lower strain in comparison with porous implants at lower half (positions 6 to 11). It depicted better osseointegration at the bottom half of porous implants than the non-porous solid implants. Obviously, it would help to provide better stability in the long run. However, it was also noticed that for bone adjacent to the bottom half of the implant having higher percentage of porosity sometimes suffer from higher strain (>6000 micro-strain). Sometimes osteoporotic patients may be vulnerable because of this.

A position-wise non-uniformity (from top to bottom) in the strain and stress pattern was observed. Increasing trend in strain was observed for positions 1, 3, 4, 5, 9, 10, and 11 for 10% porosity; positions 2, 3, 4, 5, 6, 10, and 11 for 20% porosity and 1, 2, 4, 5, 6, and 11 for 30% porosity, for 900 micron pore size. For all implant porosities alike, the maximum strain was obtained at the apex of the implant (position 11) whereas the minimum strain was located in the upper region (position 1 or position 2). As for stress, a similar trend was observed in positions 1, 2, 3, 5, 7, 9, and

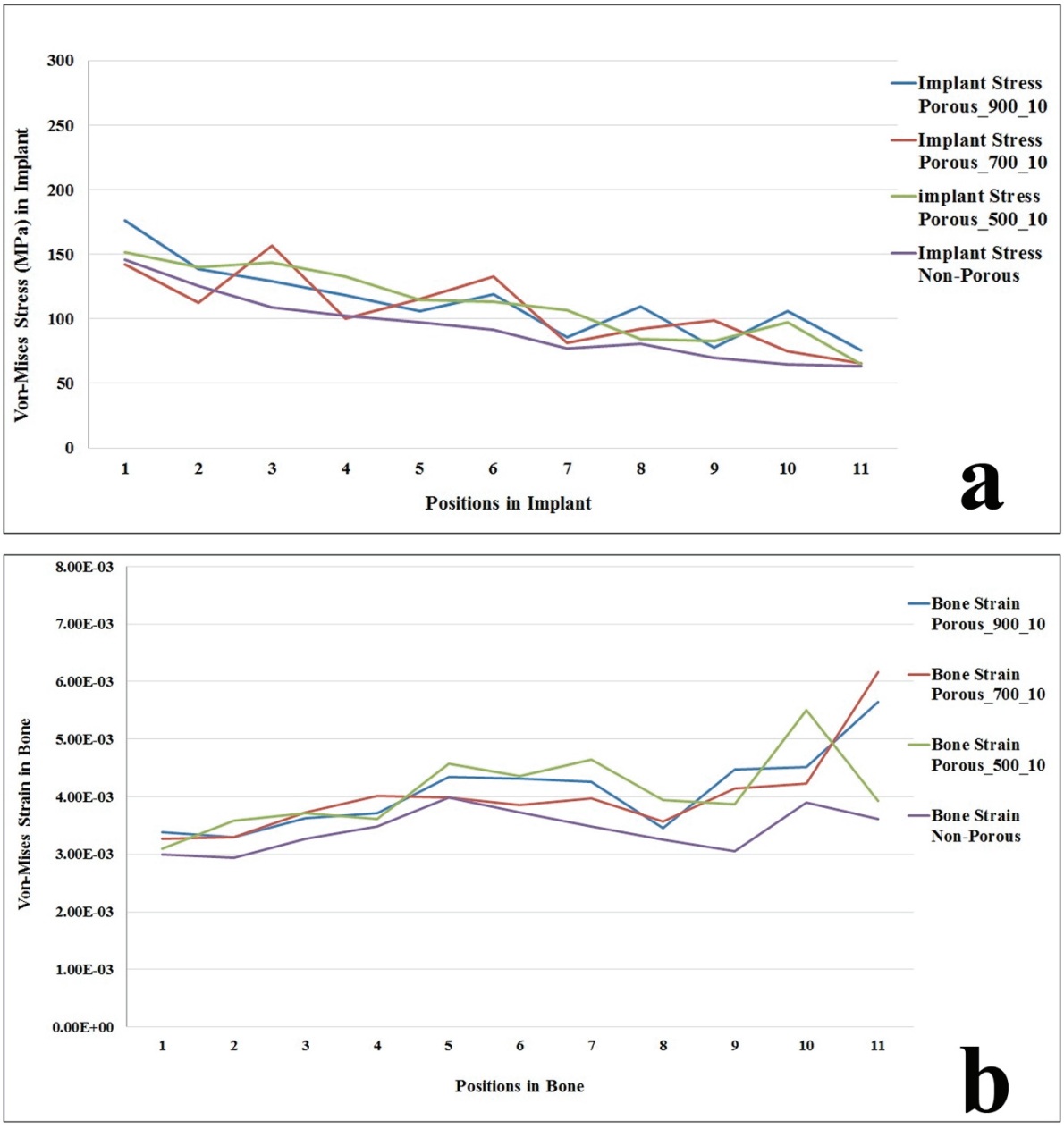

Fig. 6. For Porous_500_10, Porous_700_10, Porous_900_10 and non-porous models, (a) von Mises stress (MPa) distribution at interface on implant and (b) von Mises strain distribution at peri-implant bone

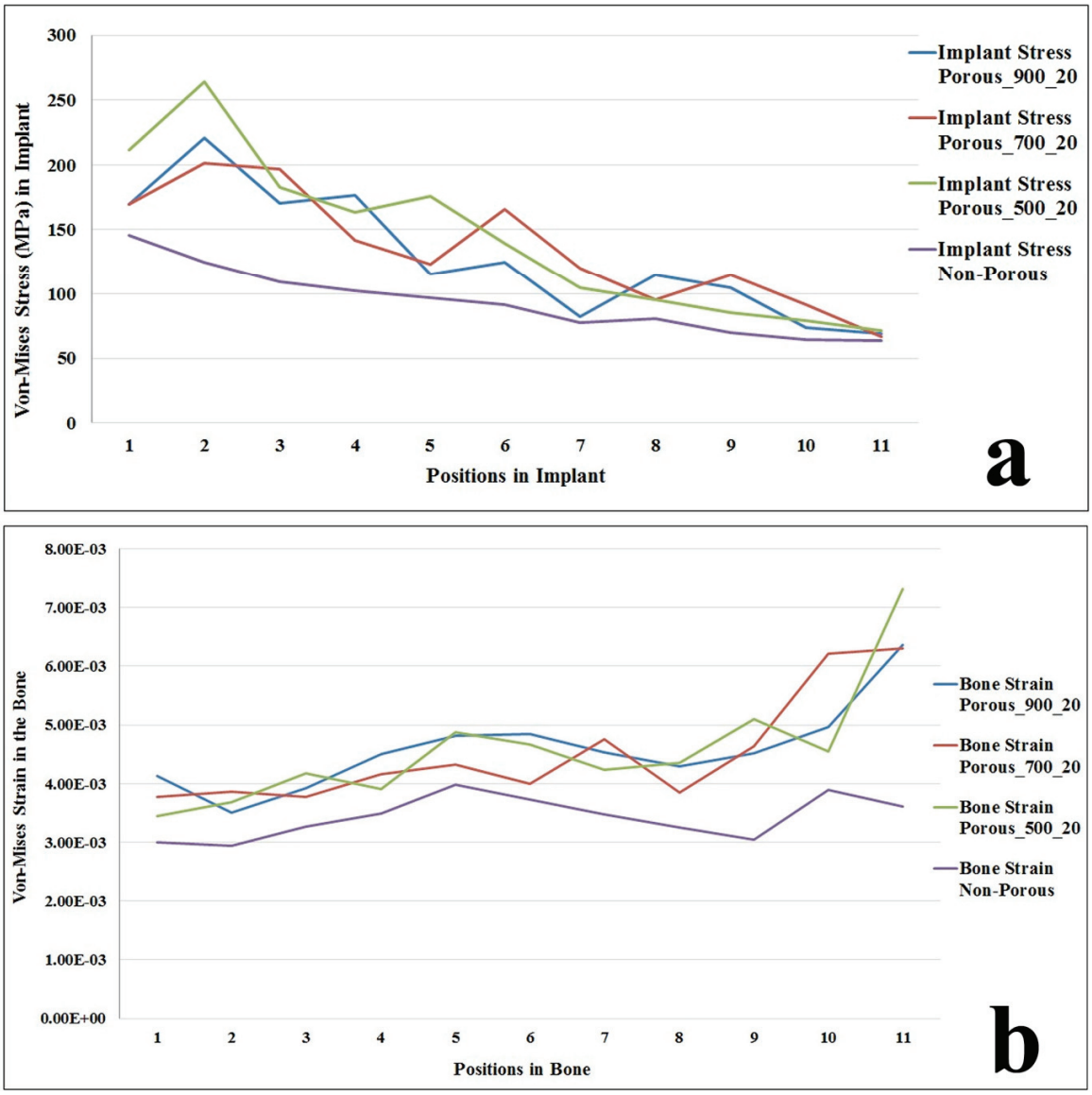

Fig. 7. For Porous_500_20, Porous_700_20, Porous_900_20 and non-porous models:
(a) von Mises stress (MPa) distribution at interface on implant and (b) von Mises strain distribution at peri-implant bone

11 for 10% porosity; positions 2, 4, 6, 8, 9, 10, and 11 for 20% porosity and 1, 2, 4, 5, 8, and 11 for 30% porosity. In this context, it is to be mentioned that the distances of selected nodes within the bone from the interface are not same for all the 11 positions but the differences were within acceptable limit (0.5 mm) (Fig. 2). Resulting from to this observations, there was a small inconsistency in the nature of stress and strain variations along the depth, as mentioned above. However, the nature of curve was very much predictable and suitable for drawing the conclusion if position-wise stress and strain plot were considered for same % porosity (Figs. 6, 7, and 8).

A major outcome that can be glanced at here is that the von Mises strain values at the interface of the bone increases uniformly with the rise in percentage porosity of the implant material. The major aim of gripping of the implant by bone is thereby served. When a systematic comparison is drawn between the non-porous model and the porous ones, it can be very well concluded that this uniformity allows for varying load to be transferred to the bone which helps in bone remodelling. But substantial increase in porosity also induces widespread decrease in strength of the implant material [21], so an optimization of the percentage porosity is very much essential for designing load bearing implants.

Stress concentration, which proportionally increases with pore size, is one of the most important criteria to avoid failure. On the other hand, it is observed that keeping the volume fraction constant, larger pore size generates more favourable mechanical condition at the

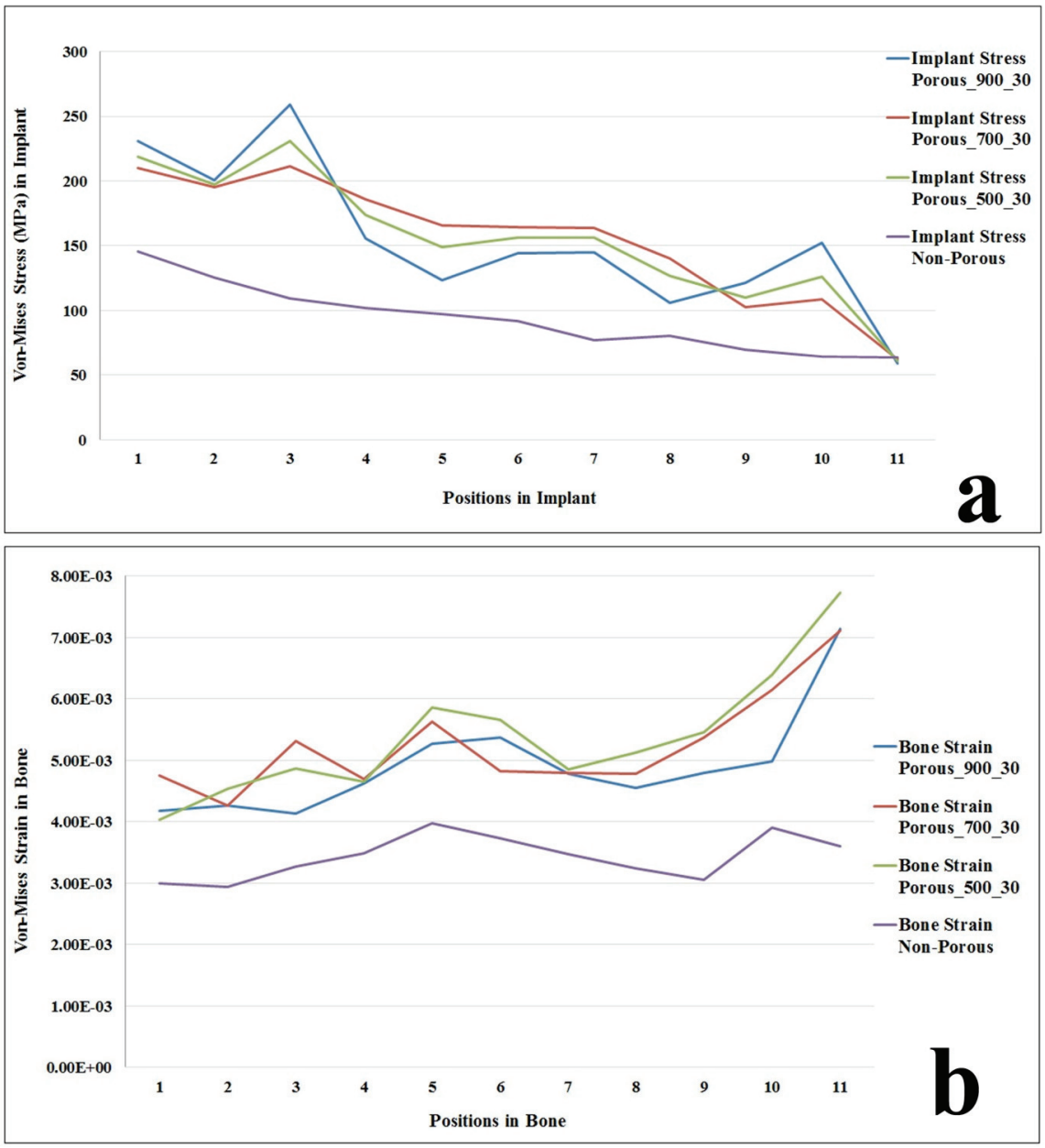

Fig. 8. For Porous_500_30, Porous_700_30, Porous_900_30 and non-porous models:
(a) von Mises stress (MPa) distribution at interface on implant and (b) von Mises strain distribution at peri-implant bone

bone–implant interface. An analogy about the above facts is presented with the help of the Fig. 9. Hence, the best possible implant for the given bone condition is the 700_30 model.

Our study is very similar to the study of Demenco et al. [6] and Roy et al. [20] for solid implants cases, but there are some small differences in modelling of screws in dimensional aspect as well as thread parameters with this study. Under 114 N compressive load, Demenco et al. [6] observed a maximum stress of 10 MPa for the bony region, whereas in the present study, maximum stress of 12 MPa, and maximum strain of 0.007 (Fig. 10) is generated under 100 N load. So there are small differences in all type of mechanical response in bone as well as implants with our study.

There are certain limitations to the approach that cannot be ignored. A static load is applied on top of the implant models, but the chewing load is dynamic in nature. The assumption that the bone is a linear material instead of a viscoelastic material has been made for simplification purpose. The advantage of this research lies in its novelty in design. The models have variable porosity (size and %) for stiffness reduction. And, by controlling the porosity, the stiffness of the implant can be controlled to make it suitable with various types of bone condition for reducing the risk of stress shielding.

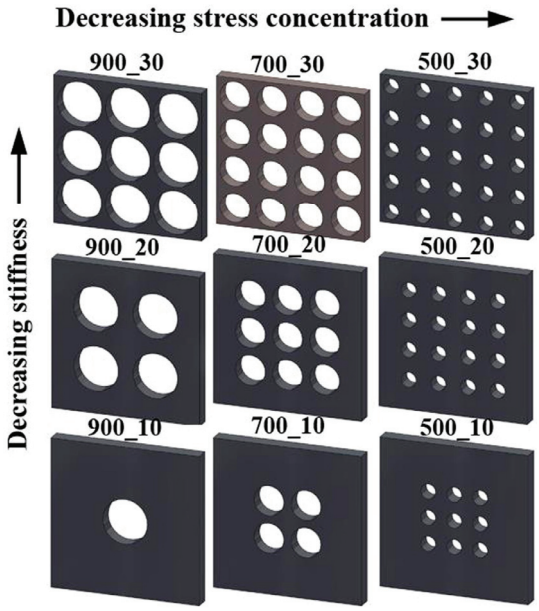

Fig. 9. Analogy of different pore size with varying % porosity

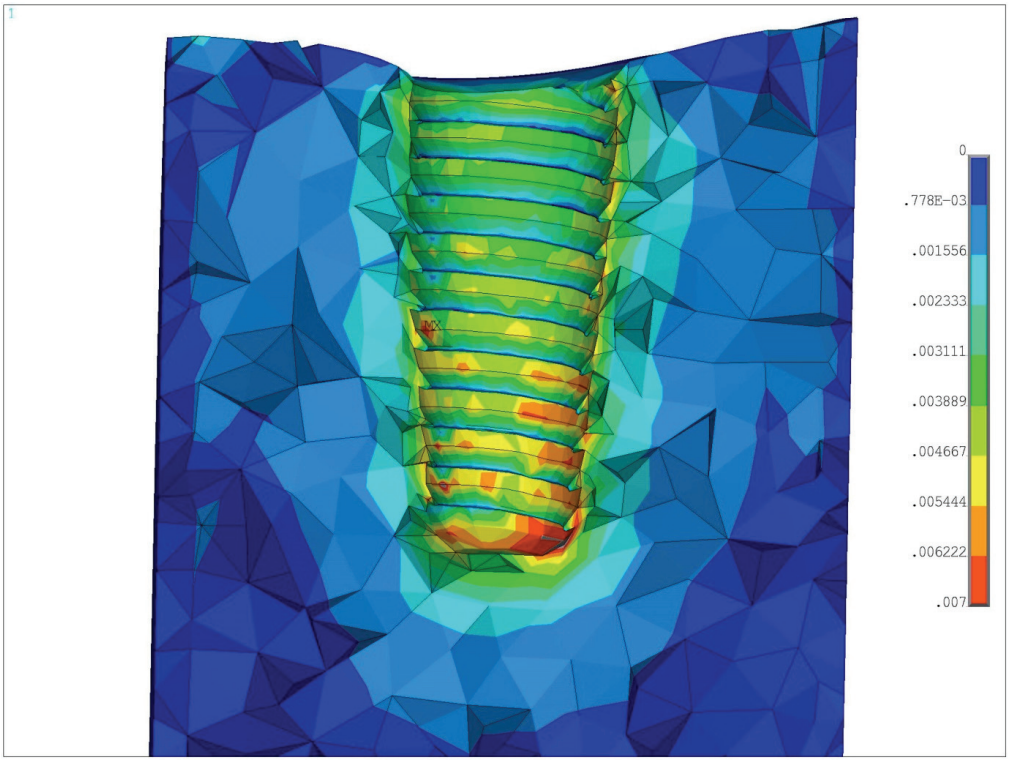

Fig. 10. Von Mises strain distribution for the bone at the interface for Porous_900_30 model

5. Conclusion

An optimum balance between the mechanical properties, porosity and pore size of the implant is to be achieved since stiffness and localised stress (stress concentration) varies as a function of porosity and pore size. This study proves that accurate and precise porous dental implants are required to ensure long-term successful implantation. Strain obtained on the peri-implant bone is on the higher side which will facilitate better bone growth. This, in turn, reduces the effect of stress shielding as the peri-implant bone takes up most of the stresses impose on the prosthesis. The strain also increased from top to bottom in the bone and the stress decreased from top to bottom for the implant at the interface. It is also concluded that smaller pore size with higher % of porosity yielded

better result in terms of stiffness reduction as well as stress concentration. The analysis may vary a lot from patient to patient depending upon the condition of bone. However, this generalized study can be utilized as a guideline for future references.

Acknowledgements

The authors thank "Translational Center on Biomaterials for orthopaedic and dental applications" sponsored by Department of Biotechnology (DBT), Govt. of India (Grant No.: DBTO0455).

References

[1] BALAZIC M., KOPAC J., JACKSON M.J., AHMED W., *Review: titanium and titanium alloy applications in medicine*, Int. J. Nano Biomater., 2007, 1 (1), 3–33.

[2] BANDYOPADHYAY A., ESPANA F., BALLA V.K., BOSE S., OHGAMI Y., DAVIES N.M., *Influence of porosity on mechanical properties and in vivo response of Ti6Al4V implants*, Acta. Biomater., 2016, 6, 1640–8164.

[3] CEHRELI M., SAHIN S., AKCA K., *Role of mechanical environment and implant design on bone tissue differentiation: current knowledge and future contexts*. J. Dent., 2004, 32, 123–132.

[4] CHLADEK W., LIPSKI T., KARASIŃSKI A., *Experimental evaluation of occlusal forces*, Acta. Bioeng. Biomech., 2001, 3 (1), 25–37.

[5] CICCIÙ M., BRAMANTI E., CECCHETTI F., SCAPPATICCI L., GUGLIELMINO E., RISITANO G., *FEM and Von Mises analyses of different dental implant shapes for masticatory loading distribution*, Oral. Implantol. (Rome), 2014, VII(1), 1–10.

[6] DEMENKO V., LINETSKIY I., NESVIT K., SHEVCHENKO A., *Ultimate masticatory force as a criterion in implant selection*, J. Dent. Res., 2011, 90 (10), 1211–1215.

[7] EL-ANWAR M.I., EL-ZAWAHRY M.M., *A three dimensional finite element study on dental implant design*, J. Genet. Eng. Biotechnol., 2011, 9, 77–82.

[8] FUKUDA A., TAKEMOTO M., SAITO T., FUJIBAYASHI S., NEO M., PATTANAYAK D.K., MATSUSHITA T., SASAKI K., NISHIDA N., KOKUBO T., NAKAMURA T., *Osteoinduction of porous Ti implants with a channel structure fabricated by selective laser melting*, Acta. Biomater., 2011, 7, 2327–2336.

[9] HORITA S., SUGIURA T., YAMAMOTO K., MURAKAMI K., IMAI Y., KIRITA T., *Biomechanical analysis of immediately loaded implants according to the "All-on-Four" concept*, J. Prosthodont. Res., 2017, 61, 123–132.

[10] IKEO N., ISHIMOTO T., SERIZAWA A., NAKANO T., *Control of mechanical properties of three-dimensional Ti-6Al-4V products fabricated by electron beam melting with unidirectional elongated pores*, Metall. Mater. Trans. A, 2014, 45(A), 4293–4301.

[11] LEE D.J., JUNG J.M., LATYPOV M.I., LEE B., JEONG J., OH S.H., LEE C.S., KIM H.S., *Three-dimensional real structure-based finite element analysis of mechanical behavior for porous titanium manufactured by a space holder method*, Comp. Mater. Sci., 2015, 100, 2–7.

[12] LIN D., LI Q., LI W., SWAIN M., *Dental implant induced bone remodeling and associated algorithms*, J. Mech. Behav. Biomed. Mater., 2009, 2, 410–432.

[13] LI J.P., DE WIJN J.R., VAN BLITTERSWIJK C.A., DE GROOT K., *Porous Ti6Al4V scaffold directly fabricating by rapid prototyping: Preparation and in vitro experiment*, Biomaterials, 2006, 27, 1223–35.

[14] MISHNAEVSKY L. JR, SABIROV I., LEVASHOV E., VALIEV R.Z., SEGURADO J., KOROTITSKIY A. et al., *Nanostructured titanium-based materials for medical implants: Modeling and development*. Mater Sci. Eng. R. Rep., 2014, 81, 1–19.

[15] MUÑOZ S., PAVÓN J., RODRÍGUEZ-ORTIZ J.A., CIVANTOS A., ALLAIN J.P., TORRES Y., *On the influence of space holder in the development of porous titanium implants: Mechanical, computational and biological evaluation*, Mater. Charac., 2015, 108, 68–78.

[16] NIINOMI M., *Mechanical biocompatibilities of titanium alloys for biomedical applications*, J. Mech. Behav. Biomed. Mater., 2008, 1, 30–42.

[17] NIINOMI M., NAKAI M., *Titanium-based biomaterials for preventing stress shielding between implant devices and bone*, Int. J. Biomater., 2011, 2011, 1–10, Article ID 836587.

[18] OTSUKI B., TAKEMOTO M., KOKUBO T., FUJIBAYASHI S., NEO M., NAKAMURA T., *Pore throat size and connectivity determine bone and tissue ingrowth into porous implants: Three-dimensional micro-CT based structural analyses of porous bioactive titanium implants*, Biomaterials, 2006, 27, 5892–5900.

[19] PENNER M.J., ALMOUSA S.A., KOLLA L., *Aseptic Loosening*, [in:] J.K. DeOrio, S.G. Parekh (Eds.), *Total Ankle Replacement: An Operative Manual*, Lippincott Williams & Wilkins, 2014, 116–122.

[20] ROY S., DAS M., CHAKRABORTY P., BISWAS J.K., CHATTERJEE S., KHUTIA N., SAHA S., ROY CHOWDHURY A., *Optimal selection of dental implant for different bone conditions based on the mechanical response*, Acta. Bioeng. Biomech, 2017, 19 (2), 11–20.

[21] ROY S., KHUTIA N., DAS D., DAS M., BALLA V.K., BANDYOPADHYAY A., ROY CHOWDHURY A., *Understanding compressive deformation behavior of porous Ti using finite element analysis*, Mat. Sci. Eng. C-Mater., 2016, 64, 436–443.

[22] TORRES-SANCHEZ C., AL MUSHREF F.R.A., NORRITO M., YENDALL K., LIU Y., CONWAY P.P., *The effect of pore size and porosity on mechanical properties and biological response of porous titanium scaffolds*, Mat. Sci. Eng. C-Mater., 2017, 77, 219–228.

[23] WAUTHLE R., AHMADI S.M., YAVARI S.A., MULIER M., ZADPOOR A.A., WEINANS H., HUMBEECK J.V., KRUTH J.-P., SCHROOTEN J., *Revival of pure titanium for dynamically loaded porous implants using additive manufacturing*, Mater. Sci. and Eng. C, 2015, 54, 94–100.

[24] ZHANG L.C., KLEMM D., ECKERT J., HAO Y.L., SERCOMBE T.B., *Manufacture by selective laser melting and mechanical behavior of a biomedical Ti-24Nb-4Zr-8Sn alloy*, Scr. Mater., 2011, 65 (1), 21–24.